POLITECNICO DI TORINO
Repository ISTITUZIONALE

Elucidating the Polymorphism of Xanthone: A Crystallization and Characterization Study

Original
Elucidating the Polymorphism of Xanthone: A Crystallization and Characterization Study / Preston, Janine Andrea; Parisi, Emmanuele; Murray, Brent; Tyler, Arwen I. I.; Simone, Elena. - In: CRYSTAL GROWTH & DESIGN. - ISSN 1528-7483. - 24:8(2024), pp. 3256-3268. [10.1021/acs.cgd.3c01506]

Availability:
This version is available at: 11583/2987801 since: 2024-04-15T06:59:56Z

Publisher:
American Chemical Society

Published
DOI:10.1021/acs.cgd.3c01506

Terms of use:

This article is made available under terms and conditions as specified in the corresponding bibliographic description in the repository

Publisher copyright

(Article begins on next page)

21 May 2024

Elucidating the polymorphism of xanthone: A crystallization and characterization study

Janine Andrea Preston[1], Emmanuele Parisi[2], Brent Murray[3], Arwen I.I Tyler[3], Elena Simone[2,3]*

[1] *School of Chemical and Process Engineering, University of Leeds, Leeds LS2 9JT, United Kingdom*

[2] *Department of Applied Science and Technology (DISAT), Politecnico di Torino, 10129 Torino, Italy*

[3] *Food Colloids and Bioprocessing Group, School of Food Science and Nutrition, University of Leeds, Leeds LS2 9JT, United Kingdom*

*Corresponding: elena.simone@polito.it

KEYWORDS: xanthone, polymorph, crystallization, polyphenol, crystal structure

ABSTRACT

The aim of this work is to shed light on the polymorphism of xanthones, a class of oxygenated molecules well-known for their bioactivity including antioxidant, anticancer, and anti-inflammatory effects. Understanding the polymorphism of xanthones can enable the design of novel solid products for pharmaceutical, nutraceutical and agrochemical applications. Prior to this work, two entries accounting for different space groups were deposited for 9-Xanthone in the

Cambridge Structure Database (CSD): an orthorhombic $P2_12_12_1$ and a monoclinic $P2_1$ structure solved at room and low temperature respectively. However, the very high similarity between these two structures and the lack of clear differences in the physical properties (e.g., thermal behavior) suggested the possibility of the existence of only one crystal structure. In fact, the differences shown in the literature data might be related to the chosen operating parameters as well as the instrumental resolution of the single crystal X-ray diffraction experiments. In the work presented here, the ambiguity in the polymorphism of xanthone is investigated using thermal analysis, powder and synchrotron single crystal XRD and optical microscopy. Additionally, a workflow for the correct identification of twinned crystal structures, which can be applied to other polymorphic systems, is presented. Such workflow combines the collection of a large dataset of high resolution diffraction patterns using synchrotron radiation with the use of principal component analysis, a dimensionality reduction technique, for a quick and effective identification of phase transitions happening during the data collection.

Crystallization experiments were designed to promote the formation of different crystal structure of xanthone was recrystallized based on past literature and beyond.

INTRODUCTION

Interest in the phenomenon of polymorphism has increased markedly in the last two decades, particularly within the pharmaceutical, advanced materials, agrochemical and even food industries [1, 2]. In foods, for instance, the cocoa butter used as the ingredient in chocolate has six reported polymorphs; each of these polymorphs could exhibit different properties in the final chocolate product (e.g., differences in melting point, sensory / organoleptic properties, thermal stability and emulsion stability)[3-6]. In organic semiconductors, different polymorphs of fused-ring

heteroaromatics could show different HOMO-LUMO bandgaps, electron/hole transport properties and topochemical reactivity [7, 8]. In pharmaceuticals, polymorph screening is considered as an irreplaceable step during the drug development process, since polymorph type could affect the stability, solubility, and bioavailability of pharmaceutical formulations [9].

Different crystal structures of the same compound can exhibit very different physical and mechanical products. Hence, establishing the solid forms landscape of a compound (including polymorphs, solvates, hydrates, co-crystals) and the transformation pathways between each of these forms is an increasingly important part of development of a new product [10-13]. Furthermore, tailoring the crystal structure of a compound in order to achieve targeted physicochemical properties is a key challenge for crystal engineers [14-17].

Solid-form screening protocols explore a wide range of crystallization strategies (e.g., solvent evaporation, cooling crystallization, crystallization from melts carried out in different classes of solvent) at a range of temperatures, pressures, and humidity levels[18]. Changes in the morphology or the presence of two or more crystal shapes in recrystallized samples are often viewed as indicators of the possible presence of polymorphs, although morphology differences for the same polymorphic form can also be observed when crystals are grown in different solvents [19]. Solid form screening can often be a difficult task, due to the occurrence of elusive or disappearing crystal structures, which are sometimes difficult to consistently isolate and characterize. Additionally, real crystals present defects and many also have structural disorder, which makes the structural characterization of these particles very challenging. Beyond our average static view of crystals (averaged positions determined by XRD, often at low temperatures), molecules are able to vibrate, change conformation and in some cases some of their groups are able to rotate. Furthermore, the quality of the crystals used to solve a structure, the choice between powder and single crystal

sampling as well as the numerical techniques applied for refinement can influence the reliability of the determined structure [20-23]. Moreover, different macroscopic phenomena (i.e. mosaicity, disorder and twinning) and experimental artifacts originating from mishandling of diffraction data can lead to erroneous definitions of new polymorphic crystal structures[24].

Marsh et al. [25] reported that the space groups of 60 crystal structures collected from single crystal measurements had been corrected and assigned to a higher Laue class than what was stated in their original papers. Müller[26] commented that the assignment of the wrong space group frequently occurs as a result of the assignment of a too low a symmetry or when structures are solved from twinned crystals. Twinning can lead to the presence of pseudosymmetry, which can either be translational or rotational [27]; pseudosymmetry is a cause of the association of wrong atom coordinates, bond lengths or interatomic distances in proposed structures. All of this generates uncertainty about the correct space group of a specific solid structure and, in turn this can lead to time and resources consuming solid product development processes. As a practical example, Karami et al.[28] discussed the reassessment of single crystal data for the compounds furosemide and finasteride: the authors found that incomplete data collections and systematic weak reflections were the cause of incorrect polymorph identification. The molecule reported in this work, was determined so far either in the orthorombic $P2_12_12_1$ space group (CSD ref Code: ZZZTXI01, ZZZTXI02 ZZZTXI011, ZZZTXI12, ZZZTXI13)[29,30,31,32,33] or as monoclinic, as shown by Trapp [34] (Form II, CSD ref code ZZZTXI14). The monoclinic structure reported by Trapp et al. [34] was solved from a twinned crystal, with very similar unit cell and crystal packing to the other known polymorph, but further details on the properties of this polymorph were not provided (e.g., melting point, solubility, biological activity). Saršūns et al. [35] even questioned the existence of Form II, considering that they were able to crystallize only the orthorhombic Form I and speculated

that Form II might result from changes in molecular orientation that could lead to the difference in packing conformation observed between the two polymorphs. They concluded that the orthorhombic form (form I) is the dominant crystalline phase (thermodynamically stable) at room temperature, while other polymorphs could be stable at different temperatures.

Given these premises, and considering that the polymorphism of xanthone is still not fully clarified, in this work we will explore it using single crystal X-ray diffraction data. Additionally, we developed a useful workflow that could be applied to other crystalline materials whose structural determination is challenging (for example other twinning crystals). Furthermore, xanthone is a flavonoid molecule of great interest for food and pharmaceutical formulators due to its antibacterial and anticancer properties [36] [37][38]. Xanthone, together with other phenolics, has also been found to exert a positive effect in the fight against obesity by preventing lipid accumulation in the liver [39].

In the work presented here, the ambiguity in the polymorphism of xanthone is investigated and a workflow for the correct identification of twinned crystal structures is presented. Xanthone was recrystallized in several solvent and operating conditions, both based on the previous literature and specifically designed for this study. To determine xanthone polymorphism, crystals were examined via synchrotron single crystal X-ray diffraction, differential scanning calorimetry and optical microscopy. Solubility in different solvents was also estimated.

MATERIALS AND METHODS

The raw material used in this work was xanthone obtained from Alfa Aesar UK (99% purity, molecular structure shown in Figure 1). The recrystallization solvents (99% purity) were all purchased from Fisher Scientific and included acetone, methanol, ethanol, and 2-Propanol (IPA),

toluene, ethyl acetate, heptane, and cyclohexane. Dimethyl sulfoxide (DMSO) and acetonitrile were purchased from Merck, UK (99% purity); whereas deionised water was obtained via a Milli-Q® water purification system, Merck, UK.

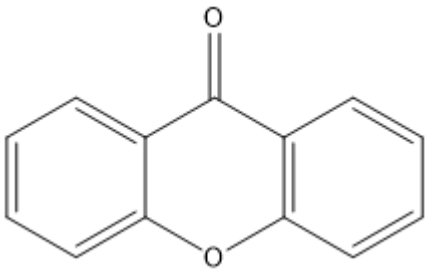

Figure 1: molecular structure of xanthone (9H-xanthen-9-one).

Solubility measurement

Solubility studies were conducted using a thermogravimetric method [40] and 10 common laboratory solvents acetone, methanol, ethanol, 2-Propanol (IPA), toluene, ethyl acetate, heptane, cyclohexane, acetonitrile and deionized water. The solvents ranged in polarity from non-polar (cyclohexane) to polar (water).

Slurries were prepared by adding excess xanthone to 10 mL of the solvent used. The vials were then placed in a temperature-controlled oven set at 20°C for a minimum of 48 hours to allow the sample to reach equilibrium. A syringe was used to take a 2 mL aliquot of solution. The extracted solution was filtered through a 0.45 µm filter and weighed into a petri dish. The petri dishes were left at room temperature for the solvent to evaporate and were weighed daily until constant mass was achieved. The solubility of xanthone was measured in the solvent mixtures outlined in Table 1: acetone: water, IPA: acetone and IPA: water solutions at different ratios. The solubility of the

xanthone was also measured in acetone: water mixtures between 20 and 50°C at 5°C intervals using the thermogravimetric method mentioned above.

Table 1: solvent mixtures used in slurry experiments to determine changes in the solubility of xanthone in mixed solvent systems.

Acetone: water	**IPA: acetone**	**IPA: water**
0:100	0:100	0:100
10:90	10:90	10:90
20:80	20:80	20:80
30:70	30:70	30:70
40:60	40:60	40:60
50:50	50:50	50:50
60:40	60:40	60:40
70:30	70:30	70:30
80:20	80:20	80:20
90:10	90:10	90:10
100:0	100:0	100:0

Recrystallization by solvent evaporation

Solid form screening of xanthone was performed using solvent evaporation in ten different solvents (water, ethanol, isopropanol, acetone, heptane, toluene, cyclohexane, methanol, ethyl acetate and acetonitrile). Three levels of initial supersaturation were used. The xanthone was weighed into 5 ml vials and 2 ml of the appropriate solvent was added to each of the vials and

stirred with an IKA® RCT Basic magnetic stirrer to dissolve the solid [38]. When the compounds had dissolved, vials were covered in parafilm with a series small holes to allow slow evaporation of the solution, as it was left at ambient temperature. The resulting crystals were filtered under vacuum and dried at room temperature.

Cooling crystallization

Recrystallization was carried out in a 300 mL jacketed vessel equipped with an overhead stirrer and a PTFE impeller to mix the system. The impeller had four pitched blades and was placed approximately 10 mm above the bottom of the vessel to ensure adequate mixing of the crystallization medium. The temperature inside the vessel was controlled by a PT-100 temperature sensor that was connected to a Huber Minstat 230 thermostat (Huber,UK), and was measured every 5 seconds. An Optek C4000 turbidity probe (Optek-Danulat GmbH) was added to monitor changes in the absorbance and transmittance throughout the crystallization experiment, so that nucleation and growth could be monitored in real time. The probe tip was orientated towards the flow of the crystallization mixture to allow representative measurements to be made and to prevent fouling phenomena. A vertical condenser was added on the top of the vessel to prevent the loss of solvent through evaporation. The stirrer was set at 200 rpm. This setting was selected because it was high enough to ensure that the xanthone particles were suspended throughout the experiment and low enough to minimize the formation of bubbles as well as crystal breakage. An overhead stirrer was used instead of magnetic agitation to reduce the rate of crystal attrition [41]. Saturated solutions of xanthone were prepared by dissolving it in specific solvent mixture (e.g., acetone: water, DMSO: water, acetonitrile: water, IPA: water) at 45°C. The solution was left stirring until complete dissolution of the solid occurred. Supersaturation was achieved by reducing the solution

temperature and nucleation was observed to occur when the solution turned cloudy and the transmittance values read by the turbidity probe started to drop significantly. The temperature was decreased from 45°C to 5°C at a rate of -1°C /min using the Huber thermoregulator. Samples were collected at the end of the crystallization experiment for analysis by optical microscopy, to observe the size and morphology of the crystals. The remaining crystals were recovered by vacuum filtration using Whatman filter paper (no.1) and air dried at room temperature for a minimum of 24 hours before analysis by scanning electron microscopy (SEM), differential scanning calorimeter (DSC) and powder x-ray diffraction (PXRD). Table 2 summarizes the ratios of acetone and water used for this set of crystallization experiments, together with the cooling rates and the loading of xanthone used for each experiment.

Table 2: Summary of the acetone:water ratios and cooling rates used to prepare xanthone crystals via cooling crystallization at 300 mL scale.

Solvent ratio w/w (acetone:water)	**Cooling rate (˚C/min)**	**Xanthone loading (g/100g of solvent)**
100:0	-1	1.60
100:0	-0.5	1.60
100:0	-0.25	1.60
100:0	-0.125	1.60
90:10	-1	1.40
90:10	-0.5	1.40
90:10	-0.25	1.40
80:20	-1	1.05

80:20	-0.5	1.05
80:20	-0.25	1.05
70:30	-1	0.71
60:40	-1	0.37
50:50	-1	0.28
50:50	-0.5	0.28
50:50	-0.25	0.28
40:60	-1	0.20

Anti-solvent crystallization

Saturated solutions of xanthone in acetone were prepared in the jacketed crystallization vessel at 45°C. Each solution was kept at 45°C long enough for the xanthone to dissolve. Then supersaturation was achieved by adding water to the solution as anti-solvent. An Anton Paar syringe pump was used to add the water to the solution at a controlled rate. The solvent ratio for acetone to water mixtures was kept constant at a weight ratio of 60:40 and the anti-solvent was added at the rates of 1.88, 3.75 and 7.50 mL/min respectively. Crystallization was allowed to continue for a further hour after the addition of anti-solvent was completed. The crystals produced were recovered by vacuum filtration and left to air dry at room temperature for a minimum of 24 hours.

High speed homogenization

A further set of experiments were conducted using an IKA T25 Ultra-Turrax high-speed homogenizer. The xanthone solutions were prepared by adding 6.4g of xanthone to 400ml of acetone (16 mg/ml) under magnetic stirring. Each solution was then transferred to a beaker, placed

under the homogenization head and agitated at 13,500 rpm. Water at room temperature was added to the stirring solution and homogenized for a further three minutes, without controlling the temperature. The samples were vacuum filtered immediately after homogenization and the crystals air-dried at room temperature for a minimum of 24 hours before analysis.

Jet homogenization

Saturated xanthone solutions were prepared in acetone at 16 mg/mL and transferred to one of the two chambers in the jet homogenization head. [42]. Water was placed in the second chamber. The amount of water used was varied to produce solvent mixture weight ratios of 50:50 and 60:40 solvent to antisolvent ratio. The solutions were passed through the high-pressure Leeds jet homogenizer (University of Leeds, UK) [43] for 1 pass at 300 bar. The samples were vacuum filtered immediately after homogenization and the crystals air-dried at room temperature for a minimum of 24 hours before analysis. All steps of the procedure were carried out at ambient temperature.

Optical microscopy particle characterization

The crystal size and shape of each sample produced in the aforementioned crystallization experiments was observed via a Bressler binocular microscope at X4, X10 and X40 magnifications and the images recorded with a Sony IMx378 Exmor RS camera (12 Mpixels and an F/20 aperture) (Sony Semiconductor Manufacturing Corp, Japan). The image data collected was analyzed using ImageJ version 1.52a [44]. For each sample, the length and width of around 700 crystals were measured and the mean aspect ratio calculated.

Scanning Electron Microscopy (SEM)

Dry crystal samples were imaged using a Benchtop scanning electron microscope (Hitachi TM3030Plus) at magnifications ranging from 100x to 6000x. Samples were arranged on Leit adhesive carbon tabs attached to SEM specimen stubs. Before measurement the prepared SEM stubs were sprayed with anti-dust spray to remove excess material that was loosely attached. The images were analyzed using image J. version 1.52a [45] . The length and width of around 700 crystals was measured and the mean crystal length and aspect ratio calculated.

Single crystal X-ray diffraction

X-ray diffraction data from a single xanthone crystal were collected on an Agilent SuperNova diffractometer at 130 K. The diffractometer was equipped with an Atlas CCD detector, which in turn was connected to an Oxford CryoStream low temperature device. The device used mirror monochromated Cu Kα radiation (λ 1.54184Å) coming from a microfocused x-ray source. The xanthone single crystal had dimensions 0.17 x 0.11 x 0.07 mm. Higher resolution data of xanthone single crystals were also collected at the X-ray diffraction beamline (XRD1) of the Elettra Sincrotrone Trieste (Italy). The crystals were dipped in NHV oil (Jena Bioscience, Jena, Germany) and mounted on the goniometer head with Kapton loops (MiTeGen, Ithaca, USA). Complete datasets were collected at different temperatures from 130 K to 300K every 10 K in order to carefully determine the polymorphic landscape of xanthone. A temperature ramp of 6 K/min was used between each step. Data were acquired using a monochromatic wavelength of 0.700 Å, on a Pilatus 2 M hybrid-pixel area detector (DECTRIS Ltd., Baden-Daettwil, Switzerland). The crystal structure was solved by intrinsic phasing using the SHELXT [46] computer algorithm, which considers the space group symmetry and peak position based on single crystal reflection data.

Further refinement of the data was performed using a least squares technique based on a full matrix (F^2) using SHELXL2016 [47]. The measured patterns were compared with the simulated powder patterns for xanthone in the CCDC Mercury software v.3.10 visualization software[48]. Additionally, a principal component analysis (PCA) was conducted on the synchrotron data to verify the presence of phase transition events in the range of temperatures analyzed. The extrapolation of PXRD diffractograms from SXRD data at the different sampling temperatures was performed by using a multi-core bilinear interpolation with CrysalisPro 42.49 [49]. MATLAB 2021a was used for the pre-processing and the analysis (using the default *pca* function). Patterns were smoothed using the Savitzky-Golay filter (default MATLAB function *sgolayfit*) with 3rd order and frame length of 7 points. The default MATLAB function *normalize* was then used to normalize data before the PCA.

Powder X-ray Diffraction (PXRD)

Powder XRD was used to characterize the xanthone samples prepared using the crystallization methods listed above (solvent evaporation, cooling and anti-solvent crystallization). A Panalytical XPERT-PRO was set up in the Bragg-Bentano mode, using Cu Kα radiation (λ= 1.54184 Å). The sample was scanned at a 2θ range between 4° to 55° (40kV, 40mA) with a step size of 0.026° and time per step of 57 s.

Differential Scanning Calorimetry (DSC)

The thermal properties of xanthone were observed using a Mettler TOLEDO DSC-1 calorimeter. The differential scanning calorimeter was calibrated using indium. The lid was crimped in place

and the samples heated from 25°C to 250°C at a rate of 10°C/min. The heat flow was measured in mW and the position of the maximum of the melting peak was used to determine the melting point.

Computational modelling

All the xanthone .cif files (ZZZTXI13, ZZZTXI14 and JP_Xanth_A60W40_twin1_hklf4) were opened in the CCDC Mercury software v.3.10 [48] and the structures reviewed to check that they contain the hydrogen atoms in the correct positions and appropriate bond types. The packing of the xanthone molecules in both the monoclinic and orthorhombic unit cells were compared. The Bravais–Friedel–Donnay–Harker (BFDH) morphology was viewed using the CSD-Materials tab and the option for Visual Habit selected. Visual Habit [49] uses the attachment energy model to calculate the predicted morphology of the crystals. The settings used for this calculation were a limiting radius of 30(Å), the Dreiding II force field and the Evjen method to calculate the electrostatic interactions. The modified morphology was viewed in the main window in Mercury. The outputs of the calculation were the total lattice energy and a breakdown of the intermolecular interactions that contribute to the lattice energy. The main facets, their % surface area and key intermolecular interactions were provided. The interactions were ranked and the main synthonic interactions identified.

RESULTS AND DISCUSSION

Solubility

Figure 2 displays the solubility of xanthone in a range of common laboratory solvents that differed in their polarities [48] . The values were determined using a thermogravimetric method and revealed that xanthone had limited solubility (< 4 mg/mL) in both highly non-polar (e.g.,

cyclohexane) and highly polar solvents (e.g., methanol and water). The highest solubility (> 12 mg/mL) was found to be in ethyl acetate, acetone and toluene that have all lower polarities (0.1-0.4) compared to water (1.0). Acetone was selected as the primary solvent for the cooling and anti-solvent experiments since this was the most cost-effective of the solvents identified previously. The limited solubility of xanthone in water made this ideal solvent to use in anti-solvent studies.

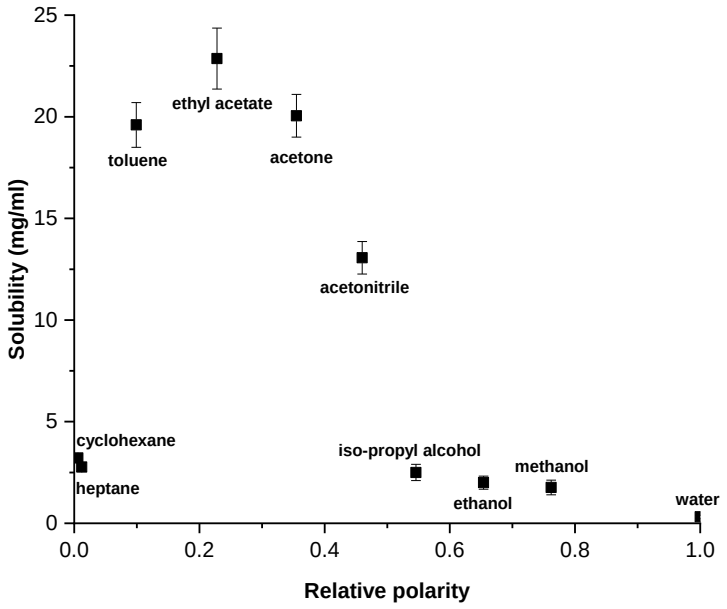

Figure 2: Summary of the solubility of xanthone at ambient temperature in common laboratory solvents

Solubility measurements were also performed for solvent mixtures to aid the design of anti-solvent crystallization experiments (Figure 3).

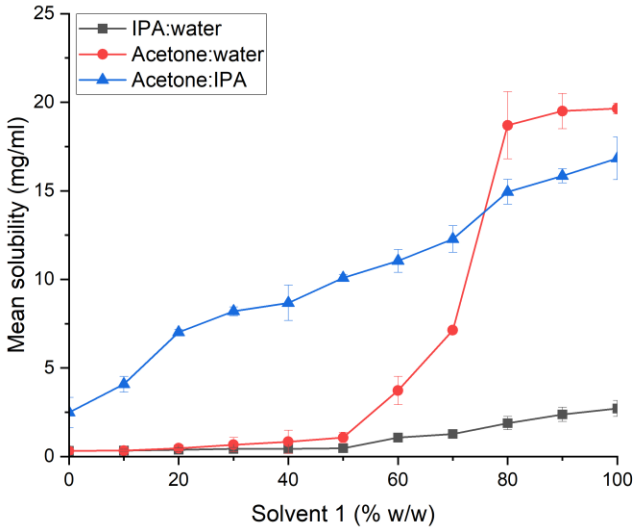

Figure 3: Solubility of xanthone at different solvent ratios (% w/w) with solvent 1 and solvent 2 for each pairing indicated in brackets a) IPA(solvent 1): water(solvent 2), b) acetone(solvent 1): IPA(solvent 2) and c) acetone(solvent 1): water(solvent 2).

Xanthone presented a high degree of solubility (> 18 mg/mL) when no water was added to the system. As the level of water increased the solubility began to reduce. The solubility drops to < 8mg/mL and < 2mg/mL when 30% and 70% w/w water are used, respectively. Solubility studies of acetone: IPA mixtures indicate that IPA does not perform well as an anti-solvent for this system. Xanthone remains more soluble in this system over the whole range of ratios investigated when compared to the same ratios with of both acetone and IPA in water. Based on these observations the acetone: water mixture was the recrystallization medium of choice because the solubility of xanthone is a strong function of the amount of acetone present. Hence, acetone: water mixtures produced the highest levels of supersaturation that can be achieved and the highest yields of crystals.

Solubility measurements as function of temperature (Supporting Information, Figure S1) revealed that as the temperature was increased from 20°C to 50°C the solubility of xanthone increased markedly in pure acetone. In mixtures of acetone and water the temperature effect was less significant and inversely proportional to the amount of water in the solvent.

Recrystallization by solvent evaporation

Xanthone crystals were successfully recrystallized from all the solvents studied except for pure water, due to the very low solubility of xanthone in this solvent. Xanthone was also very soluble in dimethyl sulfoxide (DMSO), > 25mg/ml, but this solvent was unsuitable for evaporation experiments due to its high boiling point. DMSO was therefore only used in cooling and anti-solvent recrystallizations.

Figure 4 displays the morphology of xanthone crystals recrystallized from solvents of different polarities. The crystals recovered from toluene and acetone had a needle-like morphology; whereas, crystals extracted from heptane and acetonitrile had a more prismatic shape.

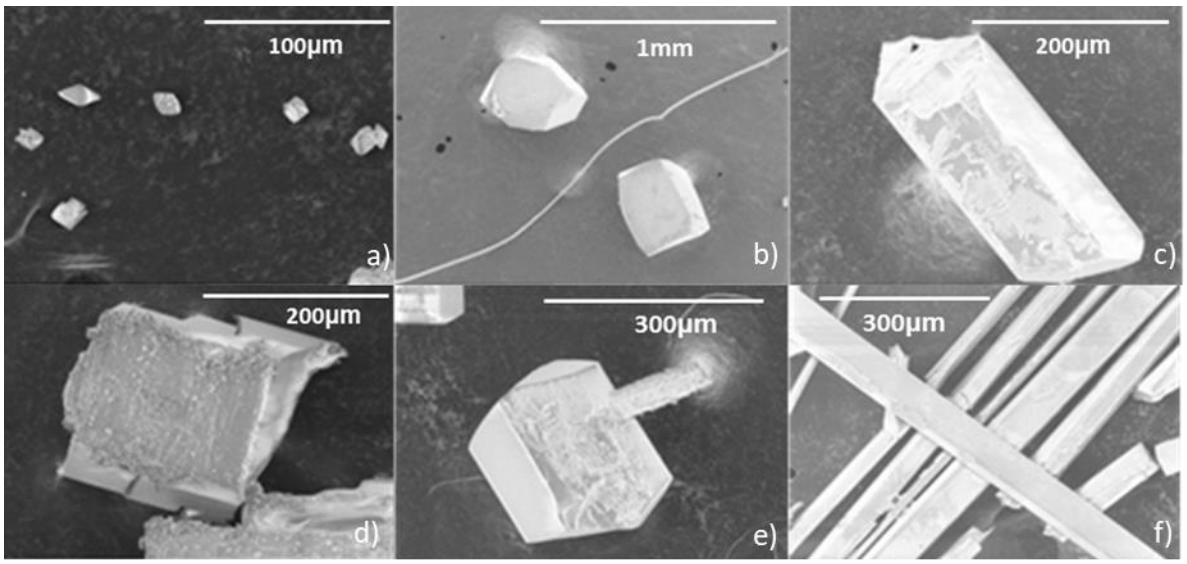

Figure 4: SEM images of xanthone crystals recrystallized from a) heptane, (b) acetonitrile, (c) ethyl acetate, (d) methanol, (e) ethanol and (f) toluene.

Despite differences in crystal shape, both powder XRD and DSC analysis (Figure 5) revealed that all the crystals were of the same solid form, irrespective of the solvent type that they were recrystallized from. This observation supports the work of Saršūns et al. [30], where only one solid-form of xanthone was crystallized at ambient temperature, via evaporation.

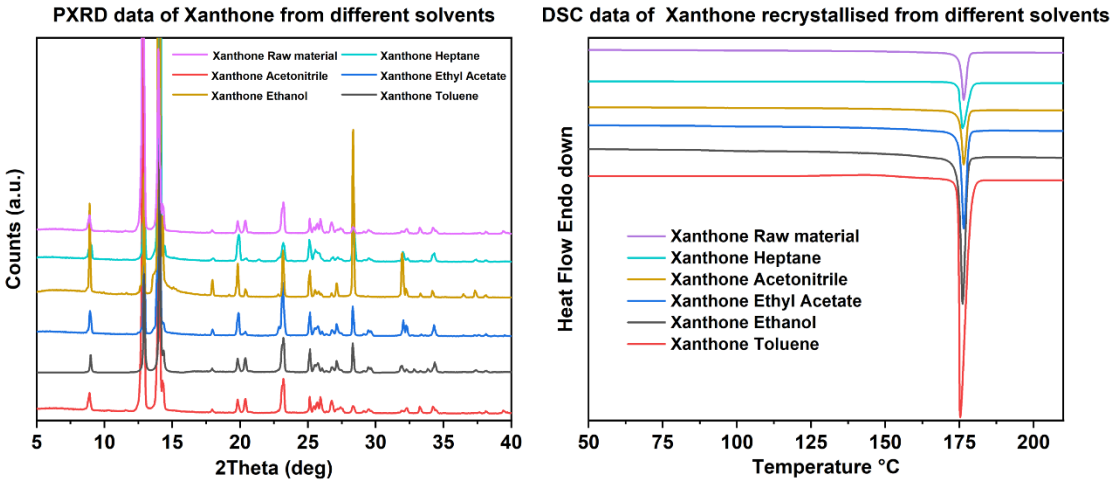

Figure 5: PXRD and DSC profiles from xanthone recrystallized from a range of solvents using the solvent evaporation technique.

Figure 6 shows the effect of different solvent mixtures on the crystal morphology. The crystal habit in the IPA-water system was the least affected by the amount of water in the solvent. The crystals had a needle-like morphology and differences in size were due to the different levels of supersaturation that could be reached with changing solvent composition; in fact, higher IPA concentrations allowed more xanthone to be dissolved before evaporation (e.g., higher solubility in IPA than water).

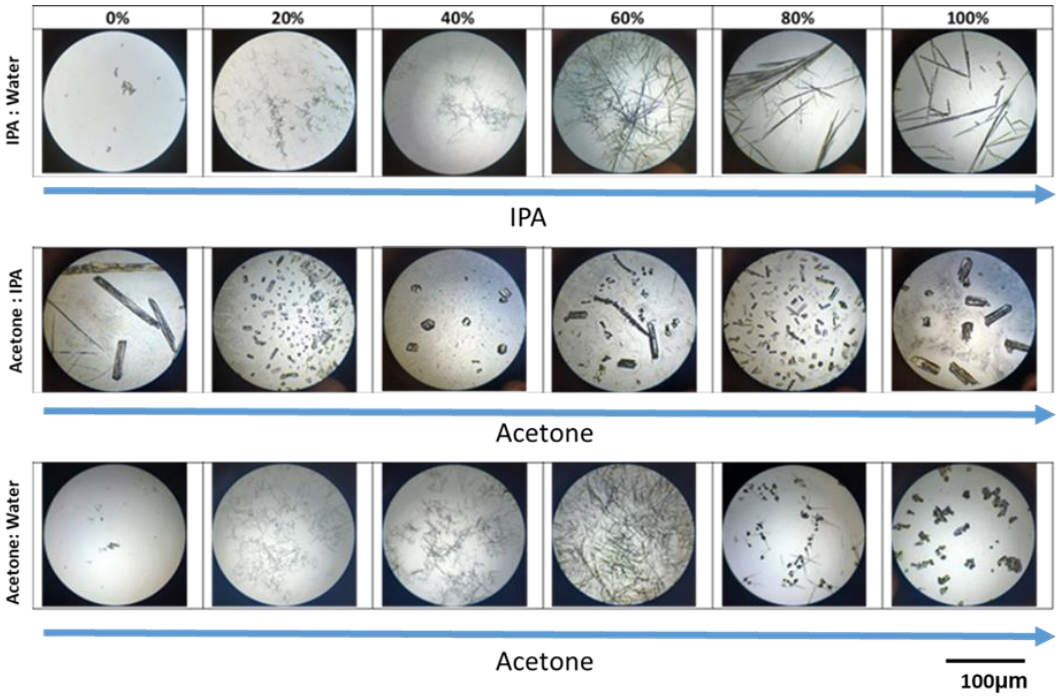

Figure 6: optical microscopy of the petri dishes containing the crystals recrystallized after the thermogravimetric analysis of xanthone in different solvent ratios of IPA: water, acetone: IPA and acetone: water.

Xanthone crystals recovered from the acetone : IPA and the acetone: water systems presented a broader shape and size distribution with rods and needles coexisting together and the presence of considerable secondary nucleation. This is probably due to the very different volatility of the two solvents that resulted in different solvent compositions during the evaporation and, hence, different solubilities and supersaturation trends over time. Such irregular supersaturation generation affected the kinetics of secondary nucleation and facet specific growth, generating the different shapes.

Cooling crystallization

Cooling crystallization was used to successfully produce xanthone rods of > 200 µm in size, due to the controlled generation of supersaturation via slow temperature decrease. Even for this set of

experiments only one polymorphic form was produced, based on PXRD and DSC analysis. The process was repeatable and routinely produced crystals of the same size and shape distributions, and solid form. Increasing the rate of cooling from −0.25°C to −1°C/minute had a limited effect on the final size distribution while the speed of filtration after the end of the experiments performed in acetone was critical in preventing further crystal growth via evaporation, as shown in Figure 7.

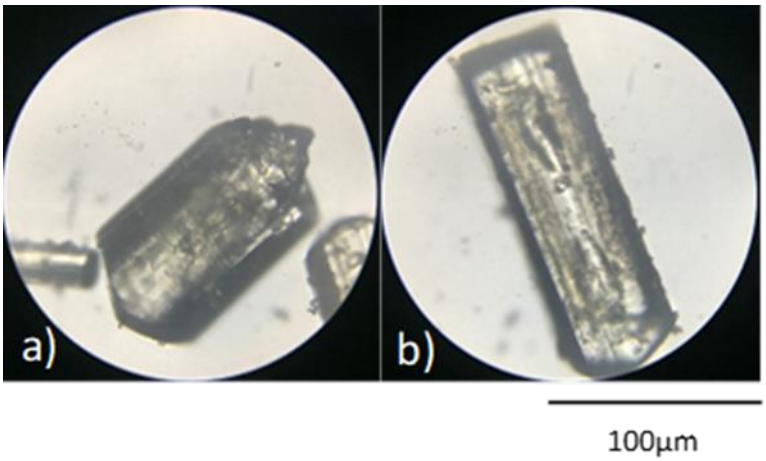

Figure 7: Effect of rate of filtration on final crystal size (crystals recovered from 100% acetone).

The effect of solvent composition on the crystals produced via cooling crystallization was also investigated. Figure 8 shows the changes in crystal morphology during cooling crystallization, when a mixed solvent system was used. DMSO:water and acetonitrile:water solvent mixtures produced crystals that were prismatic; whereas, crystals created from acetone:water mixtures were needle-like. Different, facet specific solute-solvent interactions among these solvents might be responsible for this behavior.

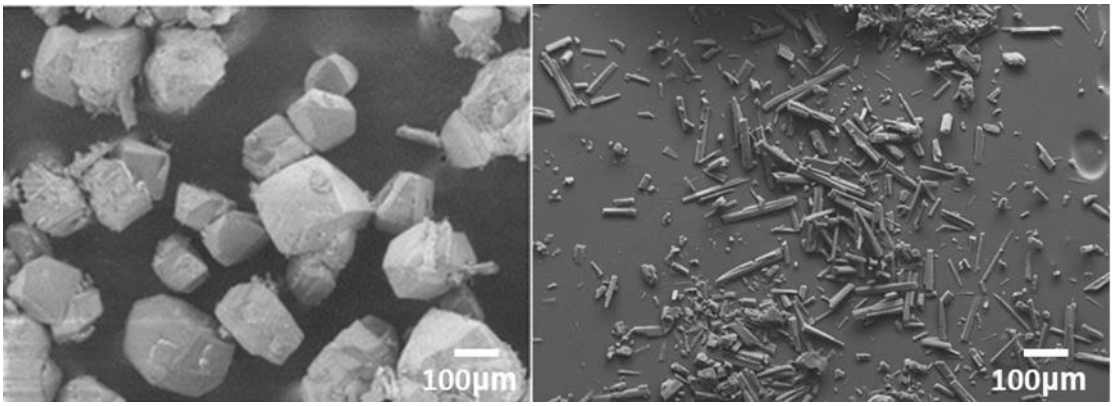

Figure 8: comparison of the prismatic crystal morphology from acetonitrile: water cooling crystallizations (left) compared to needle-like morphology recovered from acetone: water solutions (right).

Anti-solvent crystallization

Initial crystallization experiments involved the addition of pure water at different ratios to a xanthone solution in a 300 mL reaction vessel stirring at 200 rpm. Every crystallization experiment resulted in primary nucleation was successful, and began when 75% of the total water had been added. The resulting crystals were around 100 to 500 microns in size (i.e. length) and adopted either a prismatic or needle morphology depending on the ratio water to acetone. PXRD and DSC confirmed the same solid form, despite of the different morphologies achieved. It is worth noting that water in the final solvent mixture resulted in smaller and longer needles compared to higher percentages of acetone. It is worth noting that the shape and size distribution were more homogenous compared to those obtained via evaporation (Figure 6); this is due to the rapid de-supersaturation, which is typical of crystallization processes with rapid antisolvent addition.

High speed homogenization

In order to further increase the supersaturation at the nucleation point and induce the formation of metastable crystal structures an Ultra-Turrax homogenizer was used to increase the mixing speed

for the anti-solvent crystallization experiments. Initial experiments using acetone: water mixtures at ratios of 70 : 30, 60 : 40 and 50 : 50 w/w demonstrated that the amount of water added had a significant effect on the aspect ratio and size of the crystals obtained (Figure 9), but not on the solid form generate (same PXRD and DSC). The crystals prepared using acetone : water at a ratio of 70 : 30 were broader in size and shape distribution and presented a more prismatic habit; whereas crystals prepared at a ratio of 50 : 50 had a higher aspect ratio and became more needle-like. The average aspect ratios estimated from SEM images were 1.8 (70 : 30) and 4.4 (50 : 50) respectively.

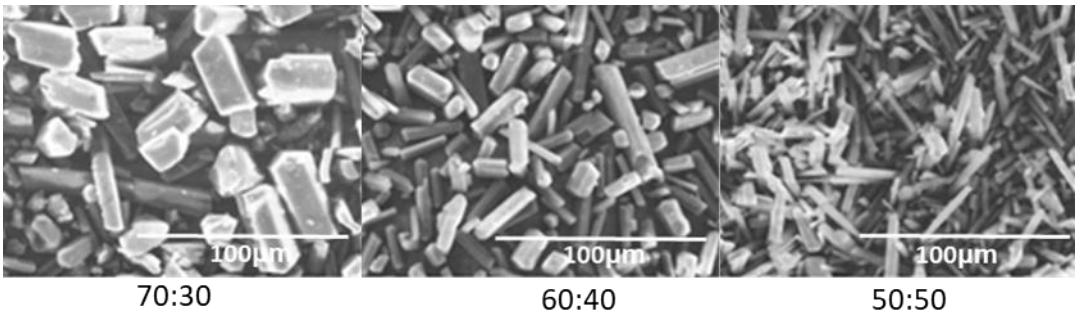

Figure 9: comparison of the aspect ratio of crystals recrystallized from acetone: water mixtures at varying weight ratio water: acetone (70:30, 60:40 and 50:50) using anti-solvent crystallization and a high speed Ultraturrax homogenizer.

Even higher water concentrations than those of Figure 9 were used (60 to 90% w/w) and the same trend was observed, despite the considerably lower solubility of xanthone in such high amount of water in the solvent mixtures. Each of the solvent ratios investigated produced crystals with a needle-like morphology and at 80 to 90% w/w water the needles became markedly thinner and shorter, the average length ranging from 5 to 30 µm. If the crystals were not filtered immediately

after preparation or the sample was filtered too slowly they continued to grow via evaporation (the average length increased even up to 50-100 μm).

Jet homogenization

The smallest crystals obtained in this work were produced via jet homogenization (around 1.3 to 20 μm of average size), possibly because this technique allowed the fastest mixing between solvent and anti-solvent, with the highest nucleation rate as high supersaturation values could be reached. The xanthone particles produced using this technique showed more variability in aspect ratio than those produced using cooling crystallization or with the Ultra-Turrax. Samples were prepared using acetone : water at ratios of 80 : 20 and 20 : 80 w/w, the resulting xanthone crystals again contained crystals of two different morphologies, prisms and needles (Table 3) but same crystal structure.

Table 3: Summary of the morphological composition (prisms and needles), mean length (and standard deviation, SD) and aspect ratio (AR) of xanthone samples prepared using 20% and 80% water

			Prisms (Size and aspect ratio (AR))		Needles (Size and aspect ratio (AR))	
Water (%)	Prisms (%)	Needles (%)	Mean length (μm)	Mean AR	Mean length (μm)	Mean AR
20	36	64	1.28 (SD ± 0.86)	1.18 (SD ± 0.22)	3.04 (SD ± 2.61)	2.93 (SD ± 2.30)
80	16	84	1.74 (SD ± 1.71)	1.25 (SD ± 0.22)	4.56 (SD ± 3.30)	3.39 (SD ± 1.64)

As shown previously for other anti-solvent experiments the percentage of the anti-solvent (water) was increased in the recrystallization medium the quantity of xanthone crystals with a prismatic

morphology decreased and the quantity of crystals with a needle morphology increased. This led to increases in the mean aspect ratios of both the prisms (from 1.18 to 1.25 (± 0.22)) and the needles (from 2.93 to 3.39 (± 1.97)) being observed. The mean crystal sizes (ie. maximum lengths) of the two morphologies were also different. The prismatic crystals were shorter in length (1.28-1.74 μm) when compared with the needles (3.04-4.56 μm).

Polymorphism investigation using single crystal XRD

Suitable single crystals of xanthone for single crystal X-ray crystallography were obtained from antisolvent crystallization from a mixture of xanthone in 60% acetone and 40% water (% w/w). The crystal structure resolution at 300 K highlights as the best solution the orthorhombic $P2_12_12_1$ space group. On cooling the same crystal to 130 K, the crystal structure resolution was different and could be described in the monoclinic space group $P2_1$ with a twinning defect. (Table S2 with crystallographic data is reported in Supporting Information). However, by comparing the twinned monoclinic structure with the orthorhombic one reported by Onuma et al. [36], it is possible to highlight how the two structures share the same intermolecular interactions, the same crystal packing, and finally the same length of crystallographic axes (Figure S3, Table S3 of Supporting Information). This is usually referred to as polysynthetic twinning, which allows the crystal to preserve its isometric shape by equalizing the displacement in every direction. This results in a *pseudopolymorphic* crystal that displays the appearance of isometric symmetry [49, 50]. This phenomenon was confirmed by the temperature ramp single crystal X-ray diffraction measurements performed at the Elettra synchrotron (Table S3). Diffraction data were obtained every 10K in the 300-129K temperature range with significantly appreciable increase in the β angle as the data collection is carried out at lower and lower temperatures. (Table S3). This

phenomenon is linked to a growing division of the diffraction spots and consequently to a better indexing of the diffraction patterns with the twinning law. (Figure S2 in Supporting Information). Here we report in Figure 10 two Ewald patterns collapsed to the lattice range of two datasets measured at 129 K and 300 K. For both datasets it was possible to index the reflection spots with two geminated cells (blue and yellow traces in Figure 10) with the following transformation matrix [100 100 001]. For the data acquired at 129K, the indexing of diffraction spots with the two geminated cells was unique. On the contrary, as the temperature increased it was possible to notice how the size of the crystallographic axes remained almost unchanged, while the 2θangle was gradually reduced from 92° to almost 90° (Table S3 of Supporting Information). For the dataset at temperature of 300 K, in which the 2θ angle is close to 90°, it is possible to index the diffraction spots with an orthorhombic cell, but with a worse figure of merit (FOM) than the monoclinic. Moreover, by solving the crystal structure via adopting the two different crystal systems it is possible to find that the discrepancy indices are very close to each other (8.6 % and 9.4%, orthorhombic and monoclinic R factor, respectively). Analysis of the data from the single crystals, combined with analyses obtained by DSC and PXRD analysis, showed the presence of a single crystal structure for xanthone at a wide range of temperatures.

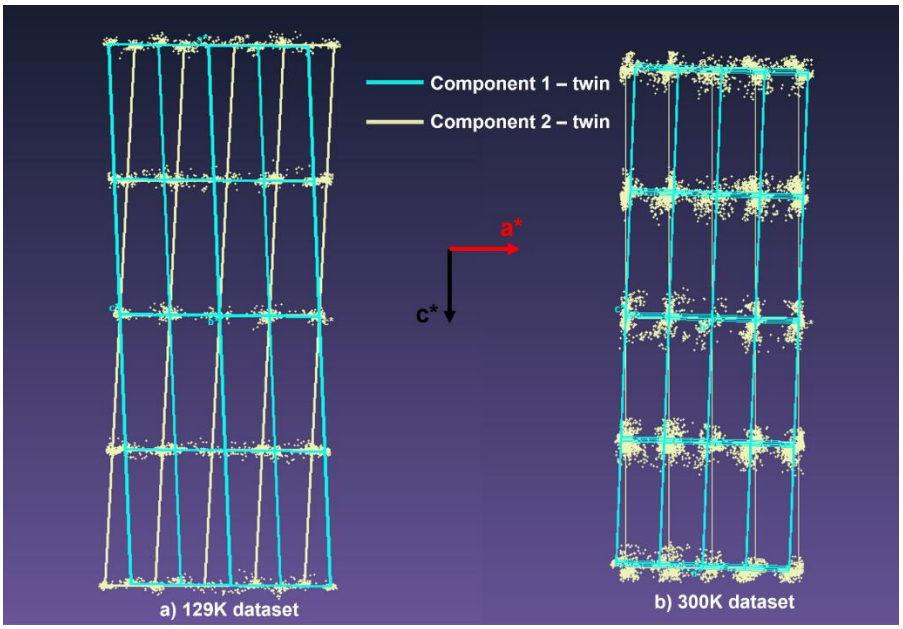

Figure 10: Ewald patterns of xanthone observed at 129K and 300K.

The data for the $P2_12_12_1$ space group can also be analyzed at a lower symmetry to give the $P2_1$ space group, which is consistent with the single crystal data in Table S1 of Supporting Information.

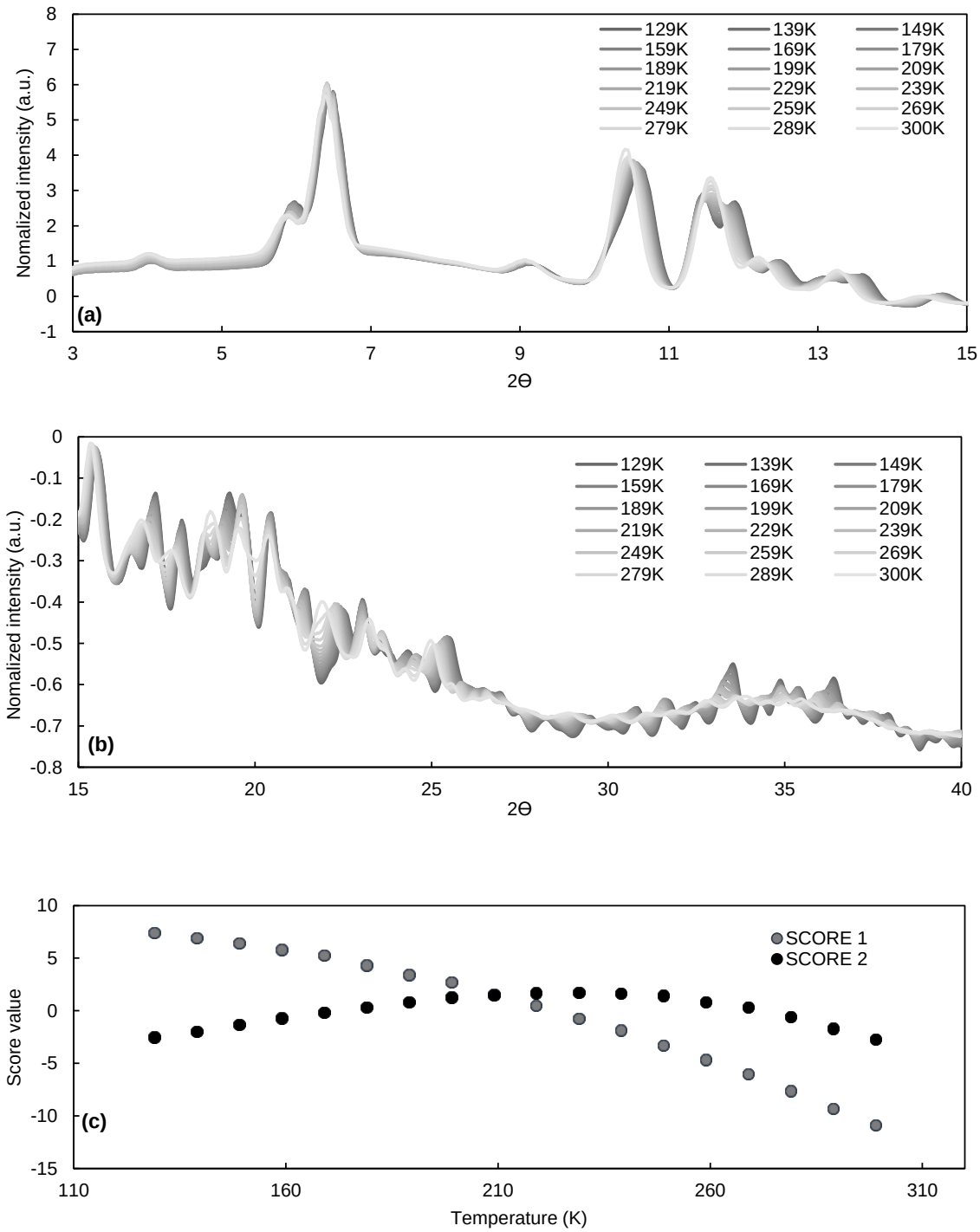

Figure 11: (a) simulated smoothed and normalized PXRD patterns from single crystal synchrotron XRD between 3 and 15° and (b) 15 to 40° 2θ (c) values of score 1 and score 2 of the PCA carried out on the data shown in (a) and (b).

The crystals are therefore monoclinic, with some weak reflections in the data leading to misidentification of the orthorhombic lattice.

In order to further verify the absence of transition events in the range of temperature studied a PCA of calculated PXRD patterns was performed on the single crystal synchrotron XRD data. Figure 11a and b show the PXRD patterns at different temperatures, where small differences are evident. Figure 11c instead shows the scores of principal components 1 and 2 at different temperatures. These two components explain 99% of the variance of the whole dataset, with score 1 explaining over 92% of the variance. Both scores do not show abrupt changes in trends as the temperature decreases, indicating the absence of a transition temperature that would indicate an enantiotropic system and, hence, the existence of two different polymorphs. Instead a non-linear dependence of the PXRD data with temperature is evident; this is likely related with the occurrence of transformation and annealing twinning, which occurs as a cooling crystal undergoes a displacive polymorphic transition.

Computational modelling

Analysis of the .cif files for the already existing ZZZTXI13 (orthorhombic), ZZZTXI14 (monoclinic) and the structure found in this work (JP_Xanth_A60W40_twin1_hklf4) revealed that all the unit cells have similar packing arrangements, similar cell dimensions (Table S3 in Supporting Information) and lattice energies of -103.9 to -104 kJ/mol respectively. These similarities are further confirmation that xanthone is monomorphic rather than polymorphic, as previously stated.

Further evidence for xanthone being monomorphic but having different crystal habits from different solvents is also indicated by the lack of quantitative data in the literature on significant differences between the two polymorphs (e.g., melting point, solubility, biological activity).

CCDC Visual Habit

Xanthone (9H-xanthen-9-one) consists of a heterocyclic fused ring system which is planar in nature. The planar conformation is stabilized by an extensive delocalized π-system [38, 39]. The two benzene rings are joined together by a central ring containing an ether group and a ketone group (Figure 1) [37, 39]. The oxygen atoms from the ketone and ether groups make hydrogen bond acceptors but there is a lack of good hydrogen bond donors on the molecule. These are principal factors to consider when studying the crystal structure and the intermolecular interactions that may occur at the surface of different facets of the monoclinic xanthone.

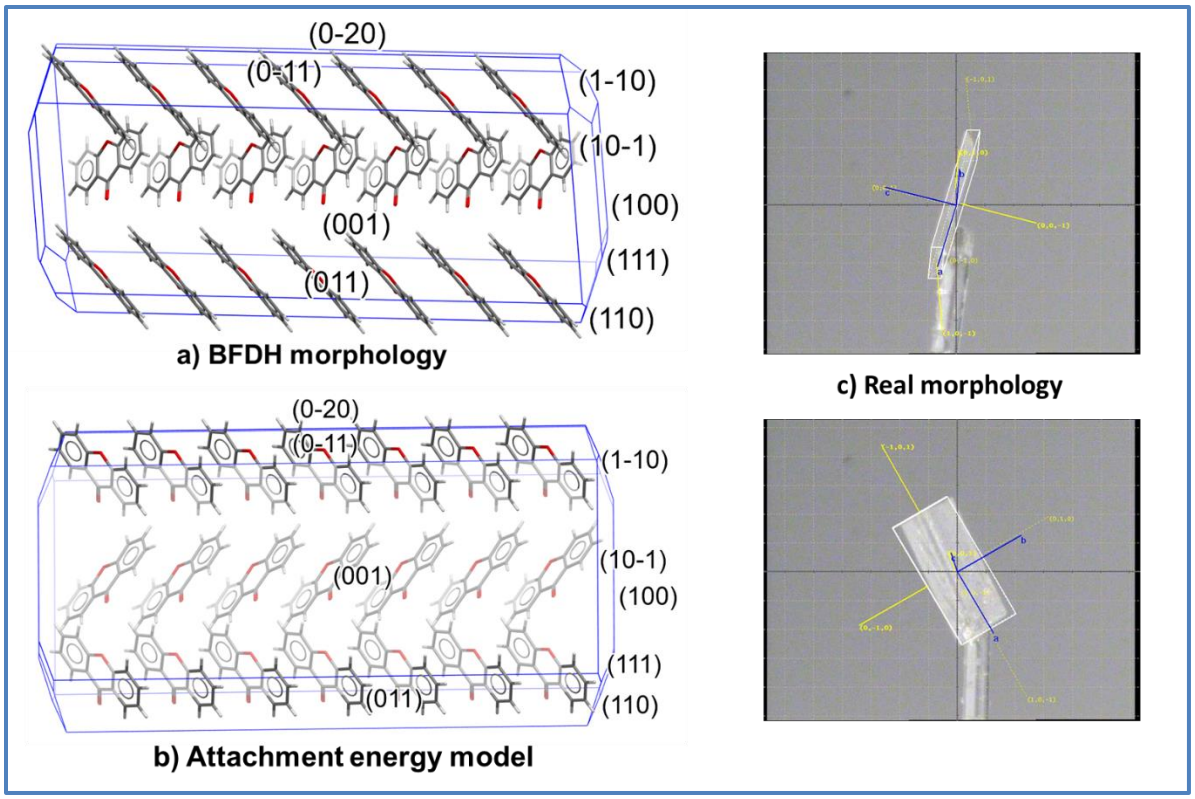

Figure 12: Predictions of the monoclinic crystal structure for xanthone crystals using a) BFDH morphology calculations and b) applying the attachment energy model using Mercury visualisation software with the Visual Habit add-on (Edgington et al., 2006; Pickering et al., 2017).

The Bravais, Friedel, Donnay Harker (BFDH) morphology [48] was used to predict the morphology of xanthone crystals. As shown in Figure 12, the predicted shape is needle-like, which is in agreement with the experimental results shown earlier. The BFDH model is the simplest model used to predict the morphology of a crystal from XRD data. It assumes that the most morphologically important facets have the greatest interplanar spacings. It considers the structure as it would be in a vacuum and does not consider the surrounding environment. It does not explain how the xanthone crystals will interact with specific solvents or more specifically which facets

will form stronger intermolecular interactions with polar solvents and which will interact more with non-polar solvents. More details about the nature and directionality of the intermolecular interactions characterizing each facet of xanthone crystals can be obtained using the attachment energy model in the Mercury tool, Visual Habit (Figure 13) [50]. The attachment energy model takes into consideration the main intermolecular interactions to build a prediction of the crystal morphology.

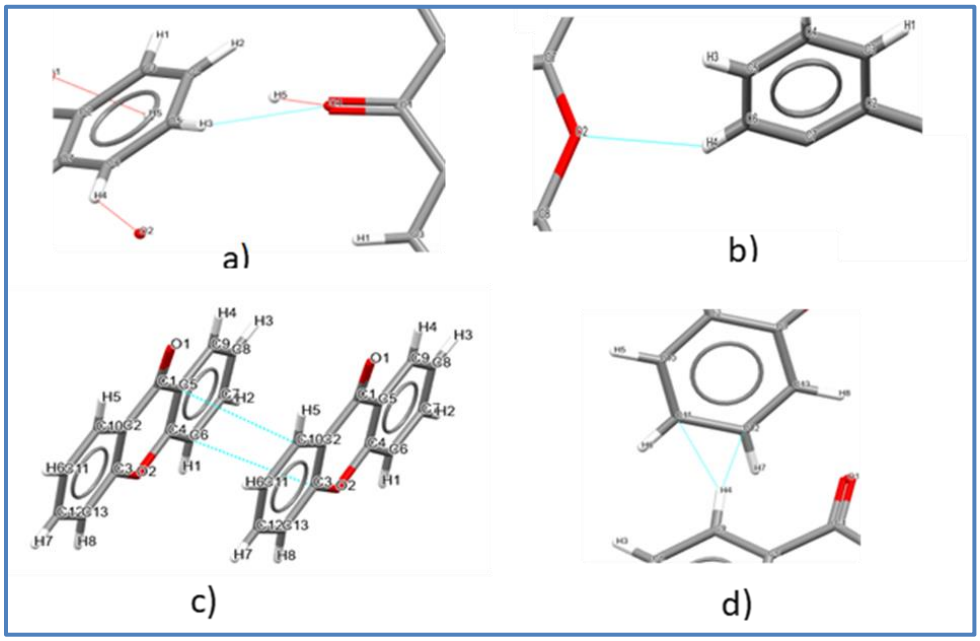

Figure 13: summary of the key synthonic intermolecular interactions of xanthone a) O on the carbonyl group → H on the aryl group, b) O from the biaryl ether group → H on the aryl group, c) π-π stacking interactions between the C atoms of aryl groups of adjacent molecules, d) van der aals attraction between aryl C atoms on one atom and the H atom on the adjacent molecule.

Figure14 displays the main intermolecular interactions of xanthone. The first point of note is that xanthone does not form hydrogen bonds and therefore all the interactions are short non-bonded

contacts. Van der Waals forces contribute 98.8% to the total lattice energy (> 80% of these interactions are due to π-π stacking interactions between the C atoms of aryl groups of adjacent molecules and the rest are due to van der Waals attraction between the aryl C atoms on one atom and the H atom on the adjacent molecule. The remaining interactions of the carbonyl or ether groups contribute little to the total lattice energy (1.2%). They are due to weak electrostatic interactions between the O on the carbonyl group and the H on the aryl group and the O from the biaryl ether group → H on the aryl group.

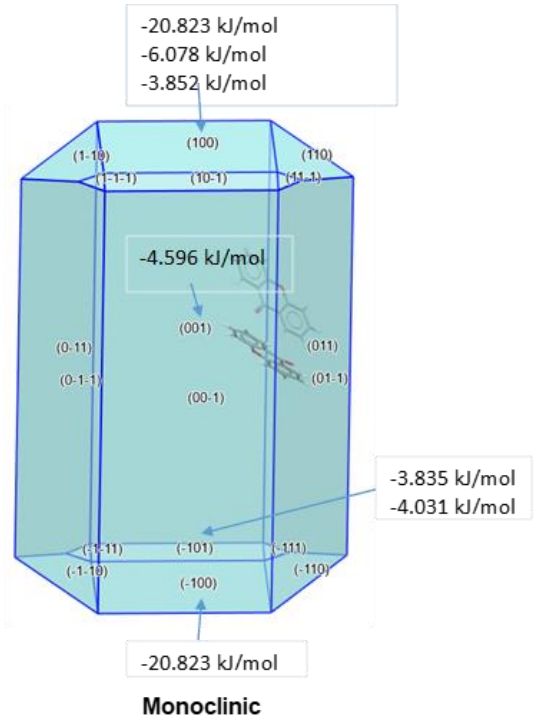

Figure 14: Summary of the contribution of different facets to the total lattice energy

The facets that grow the fastest in the xanthone crystals are the capping facets {100}, {110} and {111}. They have the highest attachment energy, principally due to the van der Waals forces, but are less morphologically important each facet contributing < 5% of the total percentage area of the crystal (Figure 14). The lateral facets {001} and {011} by contrast grow at a much slower rate and

have lower attachment energies. The latter facets are expected to interact the most with solvent molecules and be the most surface active. They have the highest density of functional groups at the surface.

CONCLUSIONS

In this paper the polymorphic landscape of xanthone was investigated and clarified. Different solvents and crystallization techniques were used in the attempt to produce metastable structures. While PXRD patterns indicated the presence of a single solid phase for all experiments, conflicting results were observed with single crystal XRD analysis carried out at ambient and low (130K) temperature. Ambient temperature measurements indicated the presence of an orthorhombic structure, while a monoclinic unit cell was better fitting the data collected at 130 K. High resolution synchrotron data collected at different temperatures and analyzed with CrysalisPro 42.49 software, Olex2 1.5 and chemometric techniques (PCA) showed the presence of only one form, the monoclinic space group, $P2_1/c$ at every temperature. The assignment of the orthorhombic space group $P2_12_12_1$ at the structures collected at higher temperatures was due to the *pseudosymmetry* effect that is due to a mis indexing of the diffraction spots with twinning unit cells. The evidence that we have presented indicates that 9H-xanthen-9-one (xanthone) is not polymorphic. Over the range of screening conditions evaluated, xanthone only forms one type of crystal lattice (i.e. monoclinic) but may exhibit different crystal habits dependent upon the preferential growth of facets in specific solvents and solvent mixtures.

ASSOCIATED CONTENT

Supporting Information: This section contains xanthone solubility in single and mixed solvent systems, crystallographic data including single crystal structure refinement, diffraction images, crystal packing and cell length and angle indexation.

The following files are available free of charge: CCDC number 2313065.

AUTHOR INFORMATION

Corresponding Author

*Dr Elena Simone, Department of Applied Science and Technology, Politecnico di Torino, Torino, Italy. Email: elena.simone@polito.it

Author Contributions

The manuscript was written through contributions of all authors. All authors have given approval to the final version of the manuscript.

Funding Sources

ERC Starting Grant 949229.

EPSRC EP/S022473/1

Elettra Sincrotrone Trieste beamtime grant 20225485

ACKNOWLEDGMENTS

This project received funding from the European Research Council (ERC) under the European Union's Horizon 2020 research and innovation programme (grant agreement no. 949229). We

acknowledge Elettra Sincrotrone Trieste (Trieste) for beamtime on beamline XRD1 under proposal 20225485. The EPSRC Centre for Doctoral Training in Molecules to Products (EP/S022473/1) is acknowledged for Janine Preston's PhD scholarship.

REFERENCES

1. Bučar, D.-K., R.W. Lancaster, and J. Bernstein, Disappearing Polymorphs Revisited. Angewandte Chemie (International ed.), 2015. 54(24): p. 6972-6993.

2. Dunitz, J.D. and J. Bernstein, Disappearing Polymorphs. Accounts of chemical research, 1995. 28(4): p. 193-200.

3. Wille, R.L.a.L., E.S. , Polymorphism of cocoa butter. J Am Oil Chem Soc, 1966(43): p. 491-496.

4. Ewens, H.M., L; Simone, E;, Analysis of the effect of recent reformulation strategies on the crystallization behaviour of cocoa butter and the structural properties of chocolate. Current Research in Food Science, 2021. 4: p. 105-114.

5. Tenorio-Garcia, E.A.-C., A; Simone ,E; Sarkar, A;, Recent advances in design and stability of double emulsions: Trends in Pickering stabilization. Food Hydrocolloids, 2022. 128: p. 1-20.

6. Metilli, L.L., A; Francis, M; Marty-Terrade, S; Ray, J; & Simone, E;, The Effect of Crystallization Conditions on the Structural Properties of Oleofoams Made of Cocoa Butter Crystals and High Oleic Sunflower Oil. Crystal Growth & Design 2021. 21(3): p. 1562–1575.

7. Bunz, U.H.F., The Larger Linear N-Heteroacenes. . Acc. Chem. Res. , 2015. 48: p. 1676-1686.

8. Centore, R.B., F; Carella, A; Causà, M; Fusco, S; Gentile, F. S; & Parisi, E; , Hierarchy of Intermolecular Interactions and Selective Topochemical Reactivity in Different Polymorphs of Fused-Ring Heteroaromatics. Crystal Growth & Design, 2020. 20(2): p. 1229-1236

9. Bauer, J.S., S.; Henry, R.; Quick, J.; Dziki, W.; Porter, W.; Morris, J., Ritonavir: An Extraordinary Example of Conformational Polymorphism. . Pharm. Res., 2001. 18: p. 859-866.

10. Klitou, P.P., C. M; Onoufriadi, L; Rosbottom, I; & Simone, E Solid-State Characterization and Role of Solvent Molecules on the Crystal Structure, Packing, and Physiochemical Properties of Different Quercetin Solvates. Crystal Growth & Design, 2020. 20(10): p. 6573-6584

11. Parisi, E.C., D; Capobianco, A; Peluso, A; Di Gaetano, S; Fusco, S; Manfredi, C; Mozzillo, R; Pinto, G; & Centore R;, Tautomeric and conformational switching in a new versatile N-rich heterocyclic ligand. Dalton Trans, 2020. 49: p. 14452–14462.

12. Steed, K.M. and J.W. Steed, Packing Problems: High Z′ Crystal Structures and Their Relationship to Cocrystals, Inclusion Compounds, and Polymorphism. Chemical reviews, 2015. 115(8): p. 2895-2933.

13. Klitou, P., Parisi, E., Bordignon, S., Bravetti, F., Rosbottom, I., Dell'Aera, M.,Cuocci, C., Chierotti, M.R., Altomare, A., & Simone, E.,, Navigating the Complex Solid Form Landscape of the Quercetin Flavonoid Molecule

Crystal Growth & Design

2023. 23(8): p. pp. 6034-6045.

14. Desiraju, G.R., Crystal Engineering: From Molecule to Crystal. Journal of the American Chemical Society, 2013. 135(27): p. 9952-9967.

15. Newman, A., Specialized Solid Form Screening Techniques. Organic process research & development, 2013. 17(3): p. 457-471.

16. Parisi, E.L., A; Fusco, S; Manfredi, C; Peluso, A; Wahler, S; Klapötke, T.M; & Centore R; , High-Energy-Density Materials: An Amphoteric N-Rich Bis(triazole) and Salts of Its Cationic and Anionic Species. Inorganic Chemistry 2021. 60(21): p. 16213–16222.

17. Parisi, E.L., A; Fusco, S; Manfredi,C; Peluso, A; Wahler, S; Klapötke, T. M; & Centore, R;, Winning Strategy toward Acentric Crystals: Transverse Dipole Moment Molecules. Cryst. Growth Des., 2023. 23: p. 4538-4544.

18. Lee, E.H., A practical guide to pharmaceutical polymorph screening & selection. Asian journal of pharmceutical sciences, 2014. 9(4): p. 163-175.

19. Chinaglia, D.L., et al., Influence of the solvent evaporation rate on the crystalline phases of solution-cast poly(vinylidene fluoride) films. Journal of applied polymer science, 2010. 116(2): p. 785-791.

20. Bobrovs, R., L. Seton, and N. Dempster, The reluctant polymorph: Investigation into the effect of self-association on the solvent mediated phase transformation and nucleation of theophylline. CrystEngComm, 2015. 17(28): p. 5237-5251.

21. Sadigh, B., L. Zepeda-Ruiz, and J.L. Belof, Metastable-solid phase diagrams derived from polymorphic solidification kinetics. Proceedings of the National Academy of Sciences - PNAS, 2021. 118(9).

22. Llinàs, A. and J.M. Goodman, Polymorph control: past, present and future. Drug discovery today, 2008. 13(5): p. 198-210.

23. Llinàs, A., et al., A new method for the reproducible generation of polymorphs: two forms of sulindac with very different solubilities. Journal of applied crystallography, 2007. 40(2): p. 379-381.

24. Bond, A.D., Boese, R. & Desiraju, G. R. , On the polymorphism of aspirin: crystalline aspirin as intergrowths of two “polymorphic” domains. . Angew. Chem. Int. Ed. , 2007. 46: p. 618-622.

25. Marsh, R.E., et al., Some 60 new space-group corrections. Acta crystallographica. Section B, Structural science, 2002. 58(1): p. 62-77.

26. Müller, U., Symmetry Relationships between Crystal Structures. Applications of Crystallographic Group Theory in Crystal Chemistry. International ed. in English ed. 2013: Oxford University Press. 332.

27. Zwart, P.H., et al., Surprises and pitfalls arising from (pseudo)symmetry. Acta crystallographica. Section D, Biological crystallography., 2008. 64(1): p. 99-107.

28. Karami, S., et al., Further errors in polymorph identification: furosemide and finasteride. Acta crystallographica. Section B, Structural science, 2006. 62(4): p. 689-691.

29. Biswas, S.C., Sen, R.K., Indian J.Pure Appl.Phys. (1969), 7, 408 CCDC (ZZZTXI01)

30. 36. Onuma, S., K. Iijima, and I. Oonishi, Structure of xanthone. Acta crystallographica. Section C, Crystal structure communications, 1990. 46(9): p. 1725-1727.nCCDC (ZZZTXI02)

31. Biswas, S.C., Sen, R.K., Indian J.Pure Appl.Phys. (1982), 20, 414. CCDC (ZZZTXI11)

32. Neng Jiang, Su-Yi Li, Sai-Sai Xie, Hequan Yao, Hongbin Sun, Xiao-Bing Wang, Ling-Yi Kong, RSC Advances (2014), 4, 63632. CCDC (ZZZTXI12)

33. Jing Tang, Shijun Zhao, Yuanyuan Wei, Zhengjun Quan, Congde Huo, Org.Biomol.Chem. (2017), 15, 1589. CCDC (ZZZTXI13)

34. Trapp, N., Vastakaite, G., Wennemers, H. CCDC 1906607: Experimental Crystal Structure Determination (ZZZTXI14). 2019. DOI: DOI: 10.5517/ccdc.csd.cc21zzgh.

35. Saršūns, K., A. Bērziņš, and T. Rekis, Solid Solutions in the Xanthone–Thioxanthone Binary System: How Well Are Similar Molecules Discriminated in the Solid State? Crystal growth & design, 2020. 20(12): p. 7997-8004.

36. Feng, Z., et al., Xanthones, a promising anti-inflammatory scaffold: Structure, activity, and drug likeness analysis. Molecules (Basel, Switzerland), 2020. 25(3): p. 598.

37. Gutierrez-Orozco, F. and M.L. Failla, Biological activities and bioavailability of mangosteen xanthones: A critical review of the current evidence. Nutrients, 2013. 5(8): p. 3163-3183.

38. Pinto, M.M.M., et al., From Natural Products to New Synthetic Small Molecules: A Journey through the World of Xanthones. Molecules (Basel, Switzerland), 2021. 26(2): p. 431.

39. Liu, Q.-Y., Y.-T. Wang, and L.-G. Lin, New insights into the anti-obesity activity of xanthones from Garcinia mangostana. Food & function, 2015. 6(2): p. 383-393.

40. Wang, Y., et al., Measurement and Correlation of Solubility of l-Valine, l-Isoleucine, l-Methionine, and l-Threonine in Water + tert-Butanol from 283.15 to 328.15 K. Journal of Chemical & Engineering Data, 2021. 66(1): p. 677-683.

41. Rychkov, D.A., S.G. Arkhipov, and E.V. Boldyreva, Simple and efficient modifications of well known techniques for reliable growth of high-quality crystals of small bioorganic molecules. Journal of applied crystallography, 2014. 47(4): p. 1435-1442.

42. Klapwijk, A.R., et al., Tuning Crystal Morphology of Succinic Acid Using a Polymer Additive. Crystal growth & design, 2016. 16(8): p. 4349-4359.

43. Lefroy, K.S., B.S. Murray, and M.E. Ries, Relationship between size and cellulose content of cellulose microgels (CMGs) and their water-in-oil emulsifying capacity. Colloids and Surfaces A: Physicochemical and Engineering Aspects, 2022. 647: p. 128926.

44. Burgaud, I., E. Dickinson, and P.V. Nelson, An improved high-pressure homogenizer for making fine emulsions on a small scale. International journal of food science & technology, 1990. 25(1): p. 39-46.

45. Abramoff, M.D., Magalhaes, P.J., Ram, S.J. , Image Processing with ImageJ. Biophotonics International, 2004. 11(7): p. pp. 36-42.

46. Sheldrick, G.M., Crystal structure refinement with SHELXL. Acta crystallographica. Section C, Structural chemistry, 2015. 71(1): p. 3-8.

47. Sheldrick, G.M., SHELXT– Integrated space-group and crystal-structure determination. Acta crystallographica. Section A, Foundations and advances, 2015. 71(1): p. 3-8.

48. Edgington, P.R., et al., Mercury: visualization and analysis of crystal structures. Journal of applied crystallography, 2006. 39(3): p. 453-457.

49. Agilent, CrysAlis PRO. (2014), Agilent Technologies Ltd: Yarnton,Oxfordshire, England.

50. Pickering, J., et al., Synthonic engineering modelling tools for product and process design. 2017: Springer.

For Table of Contents Use Only

Elucidating the polymorphism of xanthone: A crystallization and characterization study

Janine Andrea Preston[1], Emmanuele Parisi[2], Brent Murray[3], Arwen I.I Tyler[3], Elena Simone[2,3]*

[1] School of Chemical and Process Engineering, University of Leeds, Leeds LS2 9JT, United Kingdom

[2] Department of Applied Science and Technology (DISAT), Politecnico di Torino, 10129 Torino, Italy

[3] Food Colloids and Bioprocessing Group, School of Food Science and Nutrition, University of Leeds, Leeds LS2 9JT, United Kingdom

TOC:

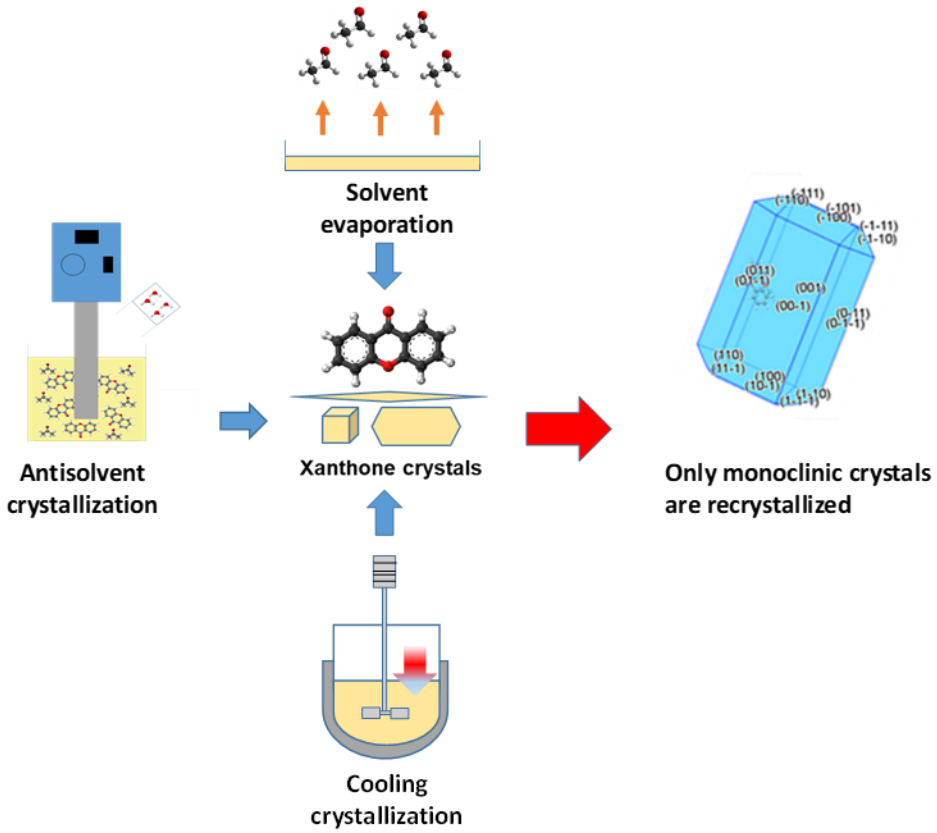

Synopsis:

Crystallographic & crystallization study on xanthone, combining synchrotron experiments and use of principal component analysis